SUPPLEMENT

QUANTIFYING HUMAN IMPACT ON THE 2018 SUMMER LONGEST HEAT WAVE IN SOUTH KOREA

Seung-Ki Min, Yeon-Hee Kim, Sang-Min Lee, Sarah Sparrow, Sihan Li, Fraser C. Lott, and Peter A. Stott

This document is a supplement to "Quantifying Human Impact on the 2018 Summer Longest Heat Wave in South Korea," by Seung-Ki Min, Yeon-Hee Kim, Sang-Min Lee, Sarah Sparrow, Sihan Li, Fraser C. Lott, and Peter A. Stott (*Bull. Amer. Meteor. Soc.*, **101**, S103–S108) • ©2020 American Meteorological Society • *Corresponding author:* Seung-Ki Min, skmin@postech.ac.kr • DOI:10.1175/BAMS-D-19-0151.2

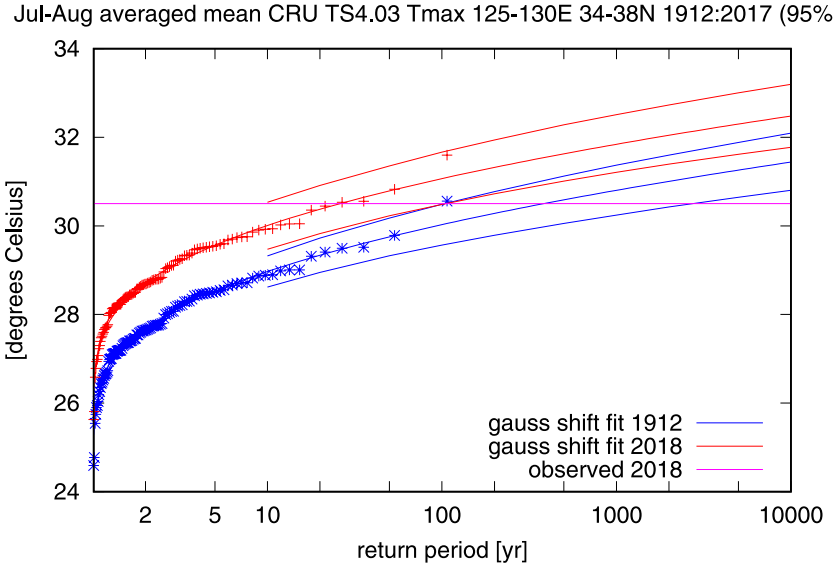

Fig. ES1. Return time plot of JA T_{max} for South Korea for 2018 (red) and for 1912 (blue) with each 95% confidence interval provided. The observed JA T_{max} obtained from CRU TS4.03 (area averages over 125°–130°E and 34°–38°N) is fitted to the Gaussian distribution with the mean linearly varying with the global mean surface temperature. The purple horizontal line indicates the 2018 JA T_{max} value. This plot is created from the public website http://climexp.knmi.nl.

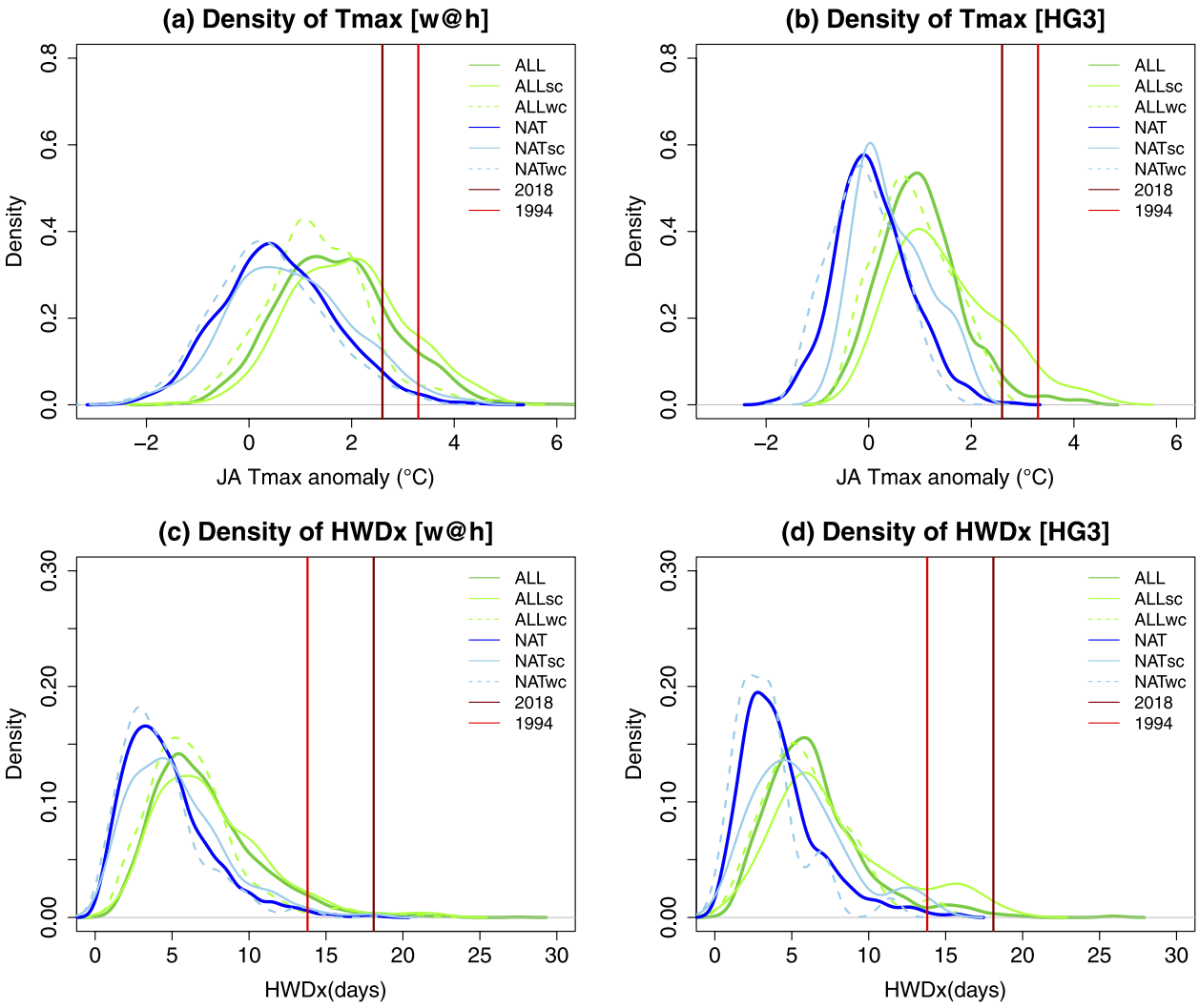

FIG. ES2. Kernel densities of (a),(b) the JA mean T_{max} anomalies and (c),(d) HWDx for ALL (green) and NAT (blue) simulations from w@h and HadGEM3-A-N216. The thick solid lines represent the results using all ensemble members while the thin solid and dashed lines indicate subsampled results from ensemble members with stronger (OLR below the 30th percentile; ALLsc and NATsc) and weaker convection (OLR above the 70th percentile; ALLwc and NATwc) over two convection zones, respectively. For HadGEM3-A-N216, precipitation is used instead of OLR. The purple and red vertical solid lines indicate the observed 2018 and 1994 values, respectively. Refer to Table ES1 and Fig. 2 for corresponding RR values and return values, respectively.

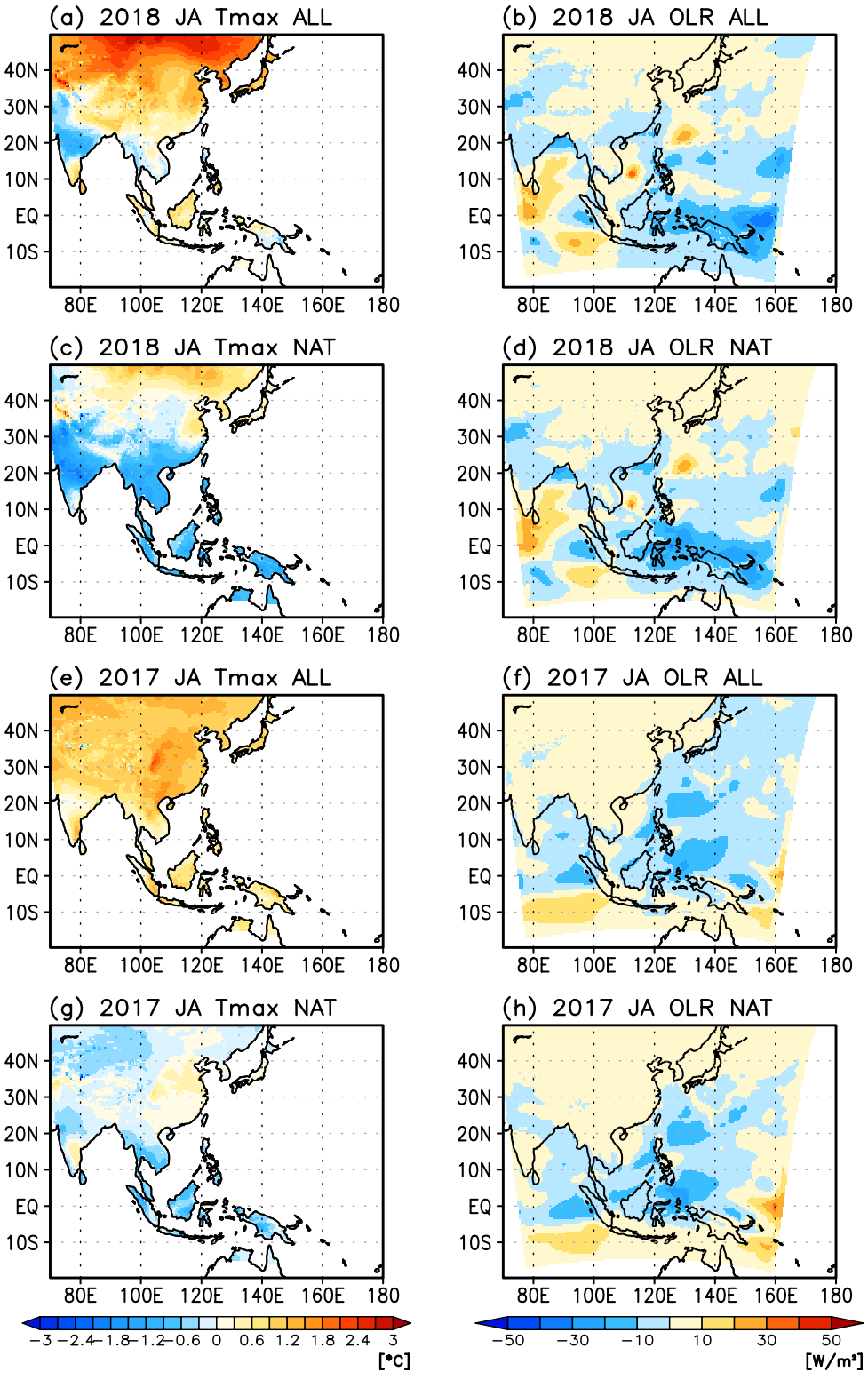

Fig. ES3. Spatial patterns of July–August (left) T_{max} and (right) OLR anomalies from the ALL and NAT simulations of w@h (upper) 2018 and (lower) 2017 experiments.

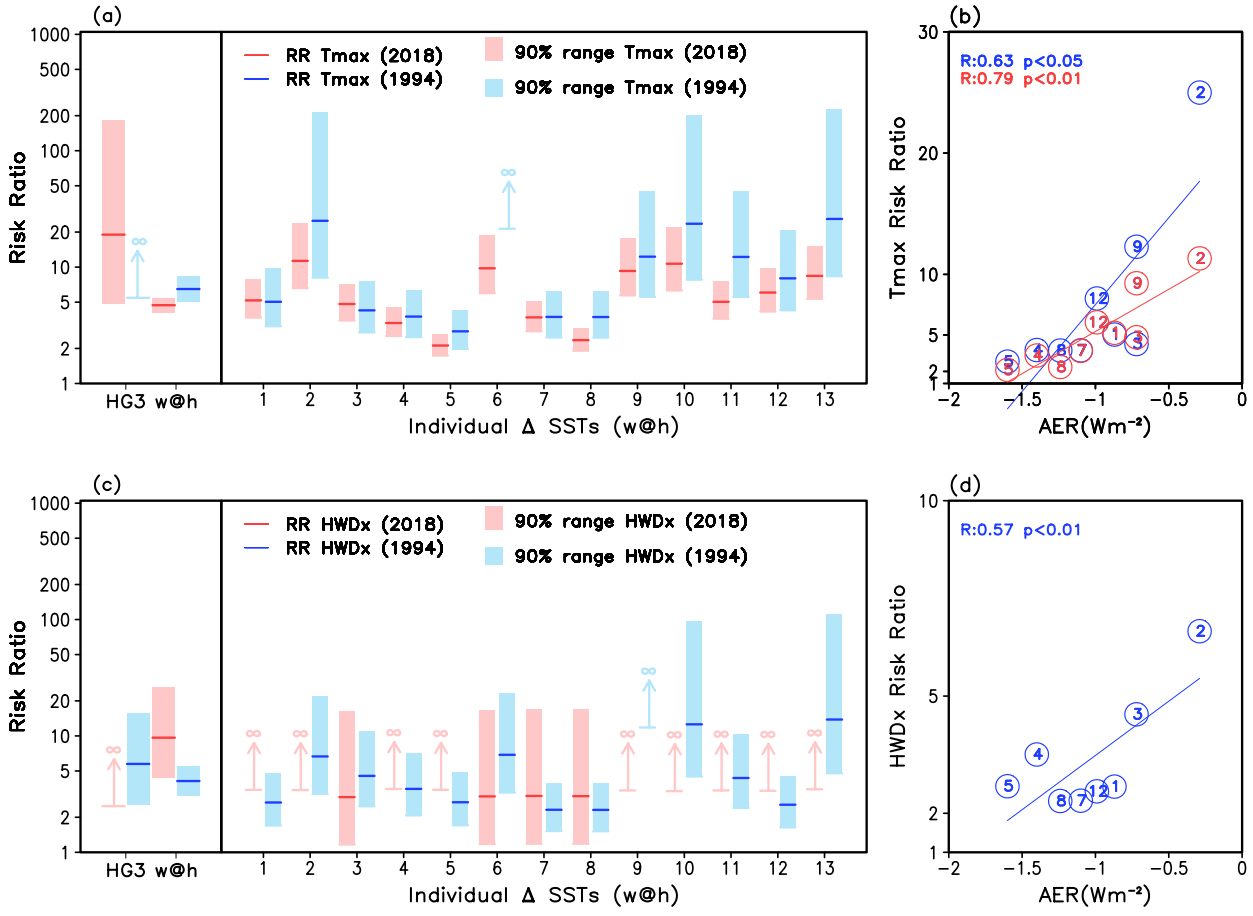

FIG. ES4. Risk ratios for (a) T_{max} and (c) HWDx from HadGEM3-A-N216 (HG3) and w@h simulations and also from w@h ensemble with different prescribed delta-SSTs (No. 1–12 obtained from different CMIP5 models and No. 13 with CMIP5 multimodel means as indicated in Table ES2). The 5%–95% confidence interval of RR is estimated using the "likelihood ratio" method (Paciorek et al. 2018). Vertical arrow depicts the infinity RR with the lower bound of confidence interval indicated. Scatterplots between aerosol forcing (AER) of CMIP5 models that provided delta-SSTs for w@h experiment [obtained from Allen and Ajoku (2016)] and corresponding risk ratios (log scale) for (b) T_{max} and (d) HWDx with intermodel correlation provided with statistical significance. Numbered circles represent values from w@h ensemble with different delta-SSTs as listed in Table ES2. Red and blue colors represent results based on the observed threshold from 2018 and 1994 values, respectively.

Table ES1. Description of weather@home (w@h) and HadGEM3-A-N216 experiments for ALL and NAT simulations, and the resulting probability (P_{ALL} and P_{NAT}) of the occurrence exceeding the observed values in 2018 JA and corresponding RR values for T_{max} and HWDx. Results from ensemble members with stronger and weaker tropical convections (top and bottom 30% selected based on OLR or precipitation anomalies averaged over the two tropical convection zones) are provided as well as those from using 1994 observations. Square brackets indicate 5%–95% uncertainty ranges of RR estimated from the likelihood ratio method (Paciorek et al. 2018).

Models (references)			w@h HadRM3P (Schaller et al. 2016)	HadGEM3-A-N216 (Ciavarella et al. 2018)
ALL simulations	External forcing		GHG: historical	GHG: historical
			Aerosols: RCP4.5 sulfate emissions	Aerosols: historical emission
			Land use/cover: historical	Land use/cover: historical
	Boundary condition		Prescribed 2018 observed SST (OSTIA; Donlon et al. 2012)	Prescribed 2018 observed SST (HadISST1; Rayner et al. 2003)
	Period		2018	2018
	No. of runs (ensemble construction)		2,300 (small perturbation to the initial potential temperature)	525 (small uniform perturbations applied to the three-dimensional temperature field)
NAT simulations	External forcing		GHG: preindustrial	GHG: preindustrial
			Aerosols: preindustrial	Aerosols: preindustrial
			Land use/cover: historical	Land use/cover: historical
	Boundary condition		Prescribed adjusted SST as observed SST minus anthropogenic influence (delta-SST; estimated from ALL minus NAT using 1996–2005 means from 12 individual CMIP5 models and multimodel mean)	Prescribed adjusted SST as observed SST minus anthropogenic influence (delta-SST; estimated from ALL minus NAT for 2018 using 19 CMIP5 models; Stone and Pall 2019, manuscript submitted to *Int. J. Climatol.*)
	Period		2018	2018
	No. of runs (ensemble construction)		3,700 [same as in ALL but using 13 delta-SST patterns; see Schaller et al. (2016) for details]	525 (same as in ALL)
JA T_{max} (2018)	All ensemble	P_{ALL}	19.8%	3.6%
		P_{NAT}	4.2%	0.19%
		RR	4.7 [4.1–5.5]	19.0 [4.9–184]
	Strong conv.	P_{ALL}	25.9%	16.7%
		P_{NAT}	7.8%	0%
		RR	3.3 [2.4–4.6]	∞ [5.0–∞]
	Weak conv.	P_{ALL}	8.2%	0%
		P_{NAT}	2.8%	0%
		RR	3.0 [1.7–5.5]	–

Table ES1. ***Continued.***

Models (references)			w@h HadRM3P (Schaller et al. 2016)	HadGEM3-A-N216 (Ciavarella et al. 2018)
JA T_{max} (1994)	All ensemble	P_{ALL}	8.7%	1.5%
		P_{NAT}	1.4%	0%
		RR	6.5 [5.1–8.4]	∞ [5.4–∞]
	Strong conv.	P_{ALL}	13.4%	4.2%
		P_{NAT}	2.6%	0%
		RR	5.1 [3.0–9.2]	∞ [0.95–∞]
	Weak conv.	P_{ALL}	4.3%	0%
		P_{NAT}	0.5%	0%
		RR	8.5 [2.9–38.0]	–
HWDx (2018)	All ensemble	P_{ALL}	1.0%	0.76%
		P_{NAT}	0.11%	0%
		RR	9.7 [4.3–26.1]	∞ [2.5–∞]
	Strong conv.	P_{ALL}	1.7%	2.1%
		P_{NAT}	0.24%	0%
		RR	7.3 [1.5–74.7]	∞ [0.32–∞]
	Weak conv.	P_{ALL}	0.78%	0%
		P_{NAT}	0.25%	0%
		RR	3.1 [0.47–34.9]	-
HWDx (1994)	All ensemble	P_{ALL}	4.7%	4.4%
		P_{NAT}	1.1%	0.8%
		RR	4.1 [3.9–5.5]	5.8 [2.6–15.6]
	Strong conv.	P_{ALL}	6.0%	12.5%
		P_{NAT}	1.7%	2.3%
		RR	3.6 [1.8–7.9]	5.4 [1.2–53.5]
	Weak conv.	P_{ALL}	3.1%	4.00%
		P_{NAT}	1.1%	0%
		RR	3.1 [1.2–9.0]	∞ [0.75–∞]

Table ES2. List of CMIP5 models that provided delta SST (ALL minus NAT using 1996–2005 means) estimates for the w@h NAT experiments as described in Table ES1. Numbers of ensemble members, aerosol sensitivity (AER; W m^{-2}), and RR values for T_{max} anomalies and HWDx are provided.

No.	Model (No. of runs)	AER	RR			
			T_{max} (2018)	T_{max} (1994)	HWDx (2018)	HWDx (1994)
1	CanESM2 (288)	−0.87	5.2	5.0	∞	2.7
2	CCSM4 (286)	−0.29	11.3	25	∞	6.7
3	CNRM-CM5 (292)	−0.72	4.8	4.3	3.00	4.5
4	CSIRO-Mk3–6-0 (301)	−1.40	3.3	3.8	∞	3.5
5	GFDL-CM3 (289)	−1.60	2.1	2.8	∞	2.7
6	GISS-E2-H (296)		9.8	∞	3.02	6.9
7	GISS-E2-R (299)	−1.10	3.7	3.7	3.05	2.3
8	HadGEM2-ES (298)	−1.24	2.4	3.7	3.04	2.3
9	IPSL-CM5A-LR (281)	−0.72	9.3	12.3	∞	∞
10	IPSL-CM5A-MR (270)		10.7	23.6	∞	12.6
11	MIROC-ESM (280)		5.0	12.3	∞	4.3
12	NorESM1-M (275)	−0.99	6.0	8.0	∞	2.6
13	Multimodel mean (297)		8.4	26	∞	13.8

REFERENCES

Allen, R. J., and O. Ajoku, 2016: Future aerosol reductions and widening of the northern tropical belt. *J. Geophys. Res. Atmos.*, **121**, 6765–6786, http://doi.org/10.1002/2016JD024803.

Ciavarella, A., and Coauthors, 2018: Upgrade of the HadGEM3-A based attribution system to high resolution and a new validation framework for probabilistic event attribution. *Wea. Climate Extremes*, **20**, 9–32, https://doi.org/10.1016/j.wace.2018.03.003.

Donlon, C. J., M. Martin, J. Stark, J. Roberts-Jones, E. Fiedler, and W. Wimmer, 2012: The Operational Sea Surface Temperature and Sea Ice Analysis (OSTIA) system. *Remote Sens. Environ.*, **116**, 140–158, https://doi.org/10.1016/j.rse.2010.10.017.

Paciorek, C. J., D. A. Stone, and M. F. Wehner, 2018: Quantifying statistical uncertainty in the attribution of human influence on severe weather. *Wea. Climate Extremes*, **20**, 69–80, https://doi.org/10.1016/j.wace.2018.01.002.

Rayner, N. A., D. E. Parker, E. B. Horton, C. K. Folland, L.V. Alexander, D. P. Rowell, E. C. Kent, and A. Kaplan, 2003: Global analyses of sea surface temperature, sea ice, and night marine air temperature since the late nineteenth century. *J. Geophys. Res.*, **108**, 4407, https://doi.org/10.1029/2002JD002670.

Schaller, N., and Coauthors, 2016: Human influence on climate in the 2014 southern England winter floods and their impacts. *Nat. Climate Change*, **6**, 627–634, https://doi.org/10.1038/nclimate2927.